Supplementary Information for

Fugitive road dust $PM_{2.5}$ emissions and their potential health impacts

Siyu Chen[1], Xiaorui Zhang[1], Jintai Lin[2], Jianping Huang[1*], Dan Zhao[1], Tiangang Yuan[1], Kangning Huang[3], Yuan Luo[1], Zhuo Jia[4], Zhou Zang[1], Yue'an Qiu[5], and Li Xie[6]

1 Key Laboratory for Semi-Arid Climate Change of the Ministry of Education, Lanzhou University, Lanzhou, 730000, China

2 Laboratory for Climate and Ocean-Atmosphere Studies, Department of Atmospheric and Oceanic Sciences, School of Physics, Peking University, Beijing 100871, China.

3 Yale School of Forestry and Environmental Studies, Yale University, New Haven, CT 06511

4 College of Earth and Environmental Sciences, Lanzhou University, Lanzhou, 730000, China

5 School of Geography and Planning, and Guangdong Key Laboratory for Urbanization and Geo-simulation, Sun Yat-sen University, Guangzhou, 510275, China

6 Gansu Provincial Maternity and Child Care Hospital, Lanzhou, 730050, China

* Corresponding author: Dr. Jianping Huang (hjp@lzu.edu.cn). Tel./Fax: 0931-8914139;.

Content:

Figure S2. The diurnal cycle of traffic volume

Figure S3. The characteristics of FRD PM_{10} emission

Figure S4. Spatial distribution of the FRD $PM_{2.5}$ concentrations

No. of Pages: 14

No. of Figure: 4

No. of Tables: 3

The FRD sample Collection and Measuring characteristics of road-deposited sediment

We collected FRD samples using a domestic vacuum cleaner (Philips FC6400) from July to November 2017 during a dry weather period and wind velocities less than 7.9 m s^{-1}. Samples were collected every 0.8 km along the length of roads longer than 2.4 km and at three random sample sites for roads less than 2.4 km (Figure S1a). At each sampling location, a rectangular sampling grid was selected, with a width of 0.5 m and a length being the width of the road (Figure S1a and c). The handheld cordless vacuum cleaner can collect road-deposited sediment conveniently (Figure S1b). Moreover, the vacuum cleaner has high efficiency to catch both fine and coarse particulates with air filtration, dust bucket, the dust separator and the cyclone. The FRD samples were preserved in numbered vacuum cleaner bags and dried at 35 °C for 7 days (Figure S1d).

We measured the value of silt loading at each sampling site by a 200-mesh sieve (<75 μm) an electronic weighting scale. And the silt loading (sL, units: g m^{-2}) is calculated as follow:

$$\mathrm{S}L = \frac{m_{total} - m_{75\mu\,\mathrm{m}}}{S} \qquad (1)$$

Where m_{total} is the mass of total FRD samples; $m_{75\mu m}$ is the mass of FRD samples lager than 75 μm; S is sampling area.

The size distribution of FRD samples was measured in laboratory. A 10-mesh sieve (<2 mm) is used to screen out leaves, scree and cigarette butts. The gross samples were divided by using coning and quartering[1]. To measure the size of dust particles more accurately, the remaining particles were further oxidized by using hydrogen peroxide solution and hydrochloric acid solution to remove potential contaminants (organic matter and calcium carbonate) from the FRD samples. And then the samples were tested by a laser particle sizer (Malvern Mastersizer, 2000) to determine the size distribution of the FRD.

Simulation of FRD $PM_{2.5}$ concentrations based on the WRF-Chem model

1. WRF-Chem model

The Weather Research and Forecasting coupled with Chemistry (WRF-Chem) mode was investigated to simulate FRD $PM_{2.5}$ concentrations in the study. Gas-phase chemical mechanisms, photolysis schemes, and aerosol schemes are coupled into the WRF-Chem model, which considers a variety of coupled physical and chemical processes such as aerosol emission, transport, deposition, aerosol interactions, chemical transport, and radiative forcing[2].

2. Model configuration

The key physical and chemical schemes used in simulations are listed in Table S2. It is noted that Peking University (PKU) emission inventory has six sectors including energy production, industry, transportation, residential & commercial, agriculture and deforestation & wildfire for CO_2, CO, $PM_{2.5}$, PM_{10}, TSP, BC, OC, SO_2, NOx, and NH_3, and polycyclic aromatic hydrocarbons[3-8]. PKU emission inventories with 0.1 by 0.1 degree spatial resolution and monthly temporal resolutions in 2014 have been included in the WRF-Chem model in this study. And FRD emission inventory is constructed in this study.

In this study, we divided the study domain into the grid of 1450 square cells with a horizontal grid interval of 500 m. The domain covered the whole urban Lanzhou in China, as shown in Fig. S3. The model atmosphere was divided into 35 vertical layers, and the top pressure of the model was 100 hPa. The simulation period was from December 15st, 2016–December 31st 2017. Only the results from the whole year in 2017 were used in this study. The initial and boundary meteorological conditions were constructed from the National Center for Environmental Prediction Final Analysis (NCEP/FNL) data at a 6 h temporal interval and 1 degree horizontal resolution. To produce a more realistic simulation, the modeled u- and v-wind components and atmospheric temperatures were nudged towards the NCEP/FNL data with a nudging timescale of 6 h.

Ground monitoring $PM_{2.5}$ Data

Daily $PM_{2.5}$ data from January to December 2017 in Lanzhou, China were obtained from the website of the China National Environmental Monitoring Center (http://113.108.142.147:20035/). Based on using the tapered elementoscillating microbalance to measure $PM_{2.5}$, the platform displays the real-time concentration of $PM_{2.5}$. This data has covered all cities at prefecture level since 2015 and has been widely used to investigate the acute health effects of ambient $PM_{2.5}$[8,9].

The diurnal cycle of traffic volume

The data of traffic volume is provided by Traffic Police Detachment of Lanzhou Public Security Bureau. The traffic volume is counted by monitors at each road intersection. Based on quality control, we get diurnal cycle of traffic volume on each road ("roads" refers to the road segment between intersections), including 45 main roads, 60 minor roads, and 55 branch roads. Compared with our observation, the data of traffic volume from monitor is reliable.

The diurnal cycle of traffic volumes on the major road, minor road, and branch road are shown in Figure S2. The traffic volumes show the lowest at 5:00 local time with average value about 250, 100, 80 vehicles h^{-1} on the major, minor, and branch road, respectively, and maintained the high value during 9:00 to 23:00 local time (LT) with dramatic increase after 7:00 local time and down at 23:00 LT. Especially, the magnitude of traffic volumes is the highest on the major road, followed by the minor road and branch road. The traffic volumes have a slight variation during the day time mainly ranging from 1000 to 2500, 800 to 1400 vehicles h^{-1} and 500 to 1000 vehicles h^{-1} on the major road, minor road, and the branch road, respectively. The high periods on three types of roads are all delayed about one or two hours on weekends compared with those on weekdays. The traffic volumes change more significantly on major roads than those on minor road, and the slight variations of traffic volumes occur on branch roads.

FRD PM_{10} emission.

The spatial distribution of FRD PM10 emission fluxes in Lanzhou is constructed in Figure S3a. The magnitude of FRD $PM_{2.5}$ emission in Lanzhou is estimated to be approximately 3216 kg d^{-1}. The FRD $PM_{2.5}$ emission fluxes are enhanced over the regions with large traffic volumes and high density of road network, predominantly in the central of the DET and the eastern of the DIT, where the value is larger than 3×10^4 μg m^{-2} d^{-1}. The FRD PM10 emission fluxes with comparatively lower values varying from 11.8×10^4 μg m^{-2} d^{-1} to 7.5×10^4 μg m^{-2} d^{-1} are occurred in the UT and ID (Figure S3a). The spatial distributions of the FRD PM_{10} emission fluxes are found to be quite similar to that of the $PM_{2.5}$ emission fluxes. The FRD emissions with the $PM_{2.5}/PM_{10}$ ratio of 0.35 can sufficiently increase the amount of fine particulate matters in urban areas, which could be suspended in the ambient atmosphere over a longer time and be more harmful for human health compared to its coarse fraction[3]. The FRD PM_{10} emission factors, as an indicator of the FRD emission ability, are sensitive factors in the construction of emission inventory. The FRD PM_{10} emission factors are approximately 3 times lager than the $PM_{2.5}$ emission factors. The interaction of large silt loading and small particle size causes high values of FRD PM_{10} emission factors in the DIT and ID, with average value of 1.13 and 0.96 g VKT^{-1}, respectively (Figure S3b). And the magnitude of FRD PM10 emission in the different UFZs decrease in the order DET (1188 kg d^{-1}) > DIT (1023 kg d^{-1}) > ID (693 kg d^{-1}) > UT (312 kg d^{-1}) (Figure S3c). The diurnal cycle of FRD PM_{10} emission is mainly consistent with variation of traffic volumes, that is, the lowest FRD PM_{10} emission occurs at 5:00 LT with value as low as 19.98 kg h^{-1} while rises dramatically to 165.42 kg h^{-1} at 11:00 LT. It maintains the high value from 8:00 to 23:00 LT accompanied by human activities, exposing citizen to high PM_{10} level (Figure S3d). Moreover, meteorological conditions also influence FRD emission as the monthly FRD PM_{10} emission is the largest (8.5×10^4 kg $month^{-1}$) in winter, followed by spring (8.0×10^4 kg month-1) and smallest (7.8×104 kg $month^{-1}$) in summer which aligns with the precipitation cycles (Figure S3e).

References:

1. Procedures for Laboratory Analysis of Surface/Bulk Dust Loading Samples; Appendix C:2; United States Environmental Protection Agency, 1993; www3.epa.gov/ttn/chief/ap42/appendix/app-c2.pdf.
2. Grell, G. A.; Peckham, S. E.; Schmitz, R.; McKeen, S. A.; Frost, G.; Skamarock, W. C.; Eder, B. Fully coupled “online” chemistry within the WRF model. *Atmos. Environ*. **2005**, 39, 6957–6975, DOI 10.1016/j.atmosenv.2005.04.027, 2005.
3. Huang, Y.; Shen, H. Z.; Chen, H.; Wang, R.; Zhang, Y. Y.; Su, S.; Chen, Y. C.; Lin, N.; Zhuo, S. J.; Zhong, Q. R.; Wang, X. L.; Liu, J. F.; Li, B. G.; Liu, W. X.; Tao, S. Quantification of global primary emissions of pm2.5, pm10, and tsp from combustion and industrial process sources. *Environ. Sci. Technol*. **2014**, 48, 13834-13843.
4. Meng, W. J.; Zhong, Q. R.; Yun, X.; Zhu, X.; Huang, T. B.; Shen, H. Z.; Chen, Y.

L.; Chen, H.; Zhou, F.; Liu, J. F.; Wang, X. M.; Zeng, E. Y.; Tao, S. Improvement of a global high-resolution ammonia emissions inventory for combustion and industrial sources with new data from the residential and transportation sectors. *Environ. Sci. Technol*. **2017**, 51 (5), 2821-2829.

5. Shen, H.; Huang, Y.; Wang, R.; Zhu, D.; Li, W.; Shen, G.; Wang, B.; Zhang, Y.; Chen, Y.; Lu, Y.; Chen, H.; Li, T.; Sun K.; Li, B.; Liu, W.; Liu, J.; Tao, S. Global atmospheric emissions of polycyclic aromatic hydrocarbons from 1960 to 2008 and future prediction., *Environ. Sci. Technol*. **2013**, 47, 6415–6424.
6. Wang, R.; Tao, S.; Ciais, P.; Shen, H. Z.; Huang, Y.; Chen, H.; Shen, G. F.; Wang, B.; Li, W.; Zhang, Y. Y.; Lu, Y.; Zhu, D.; Chen, Y. C.; Liu, X. P.; Wang, W. T.; Wang, X. L.; Liu, W. X.; Li, B. G.; Piao, S. L. High-resolution mapping of combustion processes and implications for CO2 emissions. *Atmos. Chem. Phys*. **2013**, 13, 5189-5203.
7. Zhong, Q.; Huang, Y.; Shen, H.; Chen, Y.; Chen, H.; Huang, T.; Zeng, E.; Tao, S. Global estimates of carbon monoxide emissions from 1960 to 2013. *Environ. Sci. Pollut. Res*. **2017**, 24, 864-873.
8. Chen, R.; Yin, P.; et al. Fine Particulate Air Pollution and Daily Mortality: A Nationwide Analysis in 272 Chinese Cities. *Am. J. Resp. Crit. Care.* **2017**, 196(1), 73-81; DOI 10.1164/rccm.201609-1862oc.
9. Song, C.; He, J.; et al. Health burden attributable to ambient PM 2.5 in China. *Environ. Pollu.* **2017**, 223, 575 – 586; DOI 10.1016/j.envpol.2017.01.060.
10. Philip, S.; Martin, R.; Snider, G.; et al. Anthropogenic fugitive, combustion and

industrial dust is a significant, underrepresented fine particulate matter source in global atmospheric models. *Environ. Res. Lett*. **2017**, 12(4); DOI doi.org/10.1088/1748-9326/aa65a4.

11. Chen, F.; Dudhia, J. Coupling an advanced land surface-hydrology model with the Penn State-NCAR MM5 modeling system. Part I: Model implementation and sensitivity. *Mon. Weather Rev*. **2001**, 129, 569-585; DOI 10.1175/1520-0493(2001)129< 0569:CAALSH> 2.0.CO;2
12. Hong, S. Y.; Noh, Y.; Dudhia, J. A New Vertical Diffusion Package with an Explicit Treatment of Entrainment Processes. *Mon. Weather Rev*. **2006**, 134, 2318–2341; DOI 10.1175/MWR3199.1, 2006.
13. Morrison, H.; Curry, J. A.; Khvorostyanov, V, I. A New Double-Moment Microphysics Parameterization for Application in Cloud and Climate Models. Part I: Description. *J. Atmos. Sci*. **2005**, 62, 1665–1677; DOI 10.1175/JAS3446.1.
14. Mlawer, E, J.; Taubman, S, J.; Brown, P, D.; Iacono, M.J.; Clough, S, A. RRTM, a validated correlated-k model for the longwave. *J. Geophys. Res*. **1997**, 102, 16663–16682; DOI 10.1029/97JD00237.
15. Iacono, M, J.; Mlawer, E, J.; Clough, S, A.; Morcrette, J, J. Impact of an improved longwave radiation model, RRTM, on the energy budget and thermodynamic properties of the NCAR community climate model, CCM3. *J. Geophys. Res*. **2000**, 105, 14. http://dx.doi.org/10.1029/2000JD900091.
16. Zaveri, R, A.; Peters, L, K. A new lumped structure photochemical mechanism for large-scale applications. *J. Geophys. Res*. **1999**, 104, 30387–30330,30415; DOI

10.1029/1999JD900876.

17. Zaveri, R, A.; Easter, R, C.; Fast, J, D.; Peters, L, K. Model for simulating aerosol interactions and chemistry (MOSAIC). *J. Geophys. Res*. **2008**, 113, D13204; DOI 10.1029/2007JD008782.

Table S1. The WRF-Chem configuration in this study

	Atmospheric Process	***Model Option***
Physics	*Land surface*	*Noah*
	Boundary layer	*YSU*
	Cumulus clouds	*New Grell scheme*
	Cloud microphysics	*Morrison 2-mom*
	Long-wave radiation	*RRTMG*
	Shortwave radiation	*RRTMG*
Chemistry	*Gas-phase chemistry*	*CBM-Z*
	Aerosol chemistry	*MOSAIC*
	Photolysis	*Fast-J*

Table S2. The average of $PM_{2.5}$ concentrations (unit: μg m^{-3})

UFZs[a]	Spring ([b]FRD/Total[c])	Summer (FRD/Total)	Autumn (FRD/Total)	Winter (FRD/Total)	Annual (FRD/Total)
DET	13.1/45.7	10.1/31.9	14.6/44.6	19.9/66.2	14.4/47.1
DIT	9.2/41.4	5.9/27.7	11.2/41.2	16.8/63.6	10.8/43.5
UT	6.7/38.9	3.7/25.4	7.5/37.6	12.1/58.9	7.5/40.2
ID	5.3/37.4	3.1/24.9	7.0/37.1	9.9/56.7	6.3/39.0

[a]Urban function zones: UFZs= urban function zones; DET=developed downtown; DIT=developing downtown; UT=university town; ID=industrial district; [b]FRD: the FRD $PM_{2.5}$ concentration simulated by the Weather Research and Forecasting model coupled with Chemistry (WRF-Chem) Model; [d]Total: the simulated $PM_{2.5}$ concentrations including FRD, natural dust and anthropogenic sources

Table S3. The key parameters for estimation of premature mortality

parameters	*COPD[a]*	*LC[a]*	*ALRI[a]*	*IHD[a]*	*stroke[a]*
α	*0.565*	*0.841*	*1.854*	*1.043*	*1.579*
γ	*0.019*	*0.014*	*0.002*	*0.104*	*0.013*
δ	*0.861*	*0.915*	*1.281*	*0.684*	*1.235*
C_0	*5.8*	*5.8*	*5.9*	*5.8*	*5.8*
Baseline mortality[b]	*43.8 (CI: 40.4; 49.1)*	*23.4 (CI: 17.3; 27.3)*	*28.6 (CI: 25.5; 30.6)*	*105.7 (CI: 98.8; 111.9)*	*42.3 (CI: 39.6; 48.7)*

[a]Disease: COPD= chronic obstructive pulmonary disease; LC= lung cancer; ALRI= acute lower respiratory infections; IHD= ischemic heart disease; and stroke= cerebrovascular disease; [b]Baseline mortality: CI denotes the 95% confidence intervals

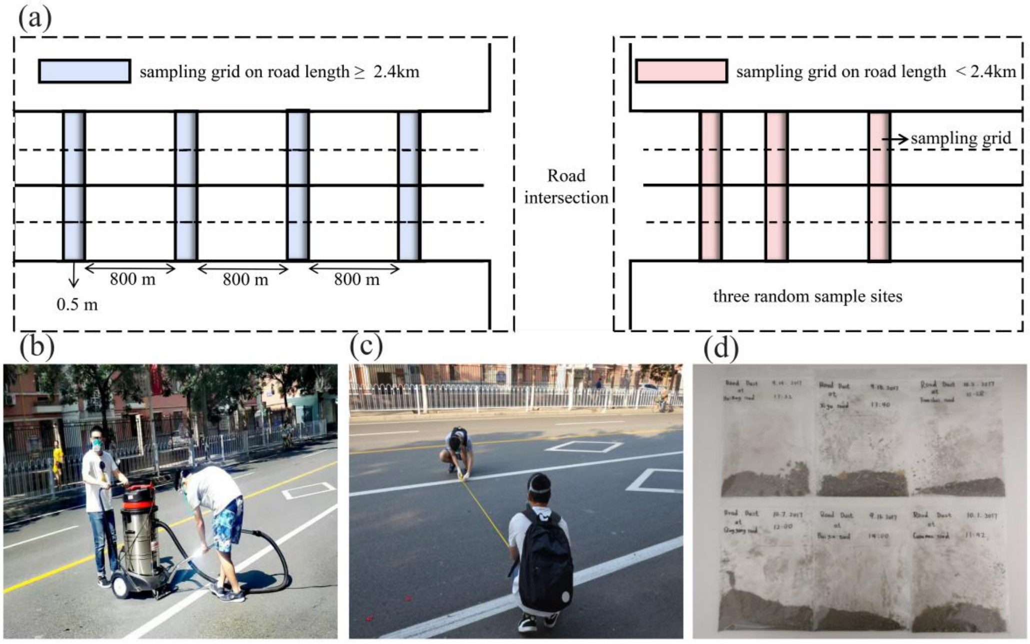

Figure S1. The process of gathering samples. (a) Sampling locations; (b) road-deposited sediments were sampled by a vacuum cleaner; (c) measuring the areas of the sampling grid; (d) FRD samples collected in vacuum cleaner bags.

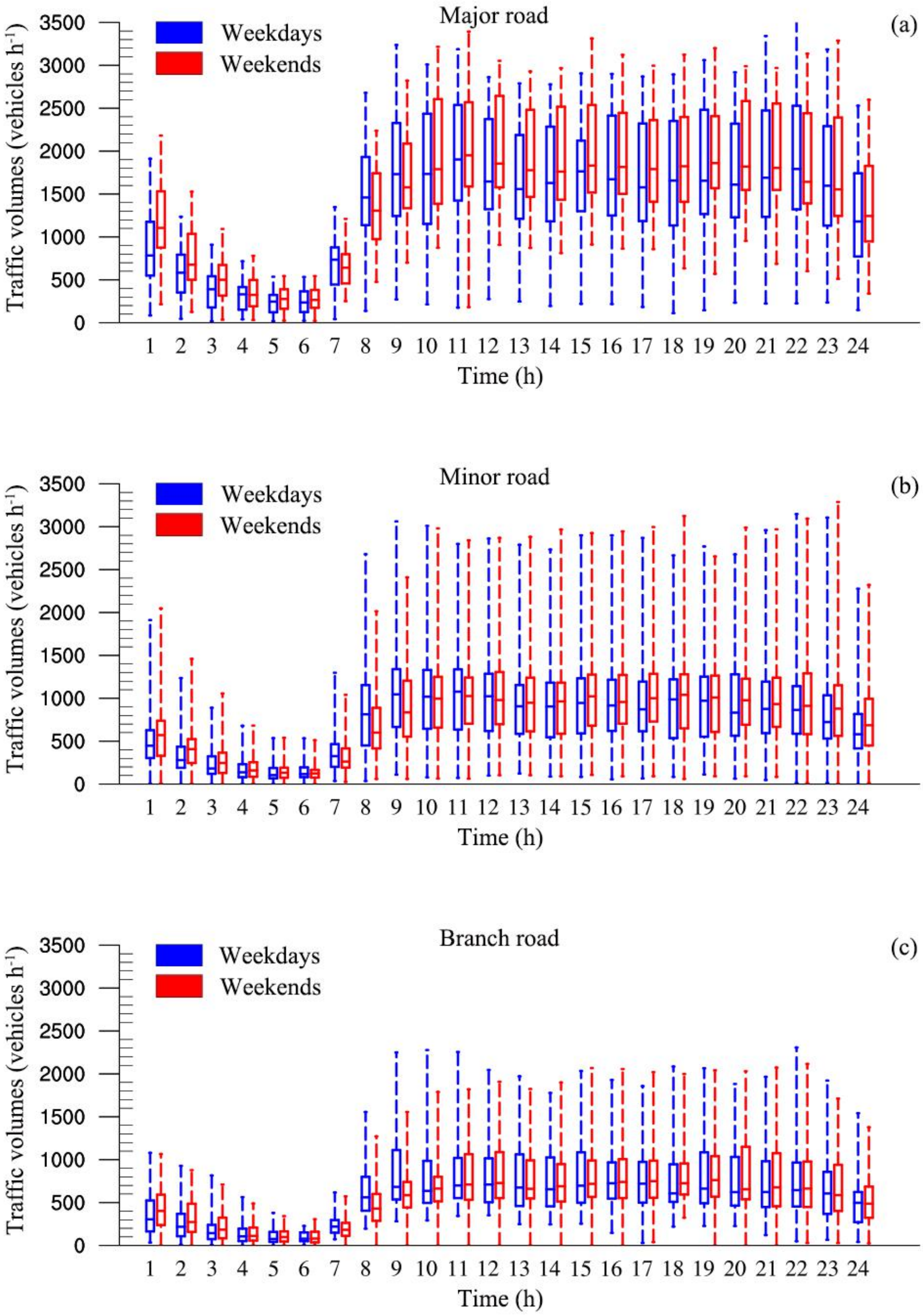

Figure S2 The diurnal cycle of traffic volume on (a) major road; (b) minor road; (c) branch road. (Dashes in the boxes denote medians of traffic volume. Opening and closing of the boxes presents 25 and 75th percentiles for each dataset. The dotted line tops of the boxes are maximum and minimum, respectively).

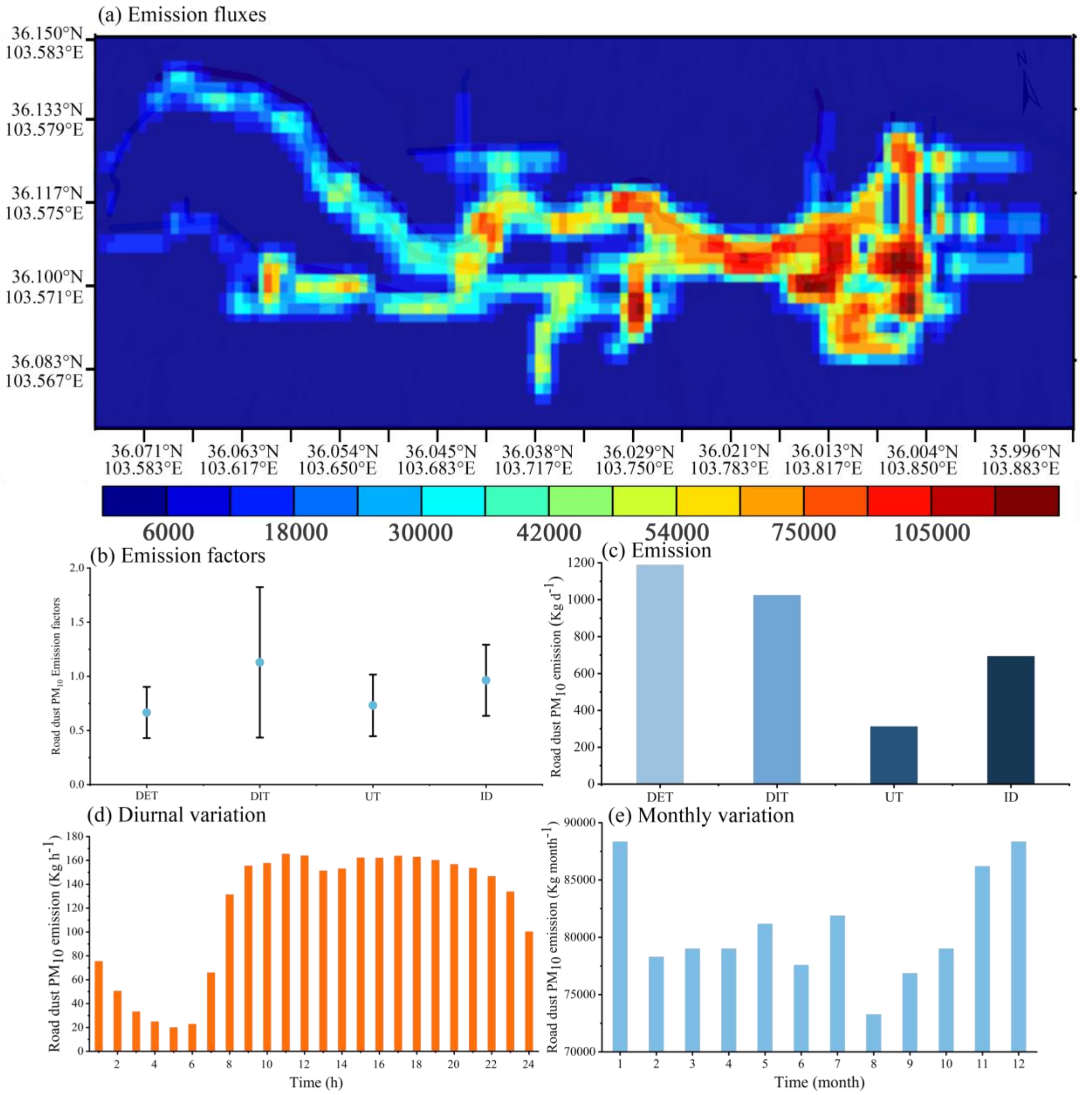

Figure S3. (a) The pattern of FRD PM_{10} emission fluxes (unit: μg m^{-2} d^{-1}); (b) emission factors (unit: g VKT^{-1}), (c) Total amount (unit: kg d^{-1}), (d) Diurnal variations (unit: kg h^{-1}), and (e) Monthly variations (unit: kg $month^{-1}$) of FRD PM_{10} emission in four UFZs.

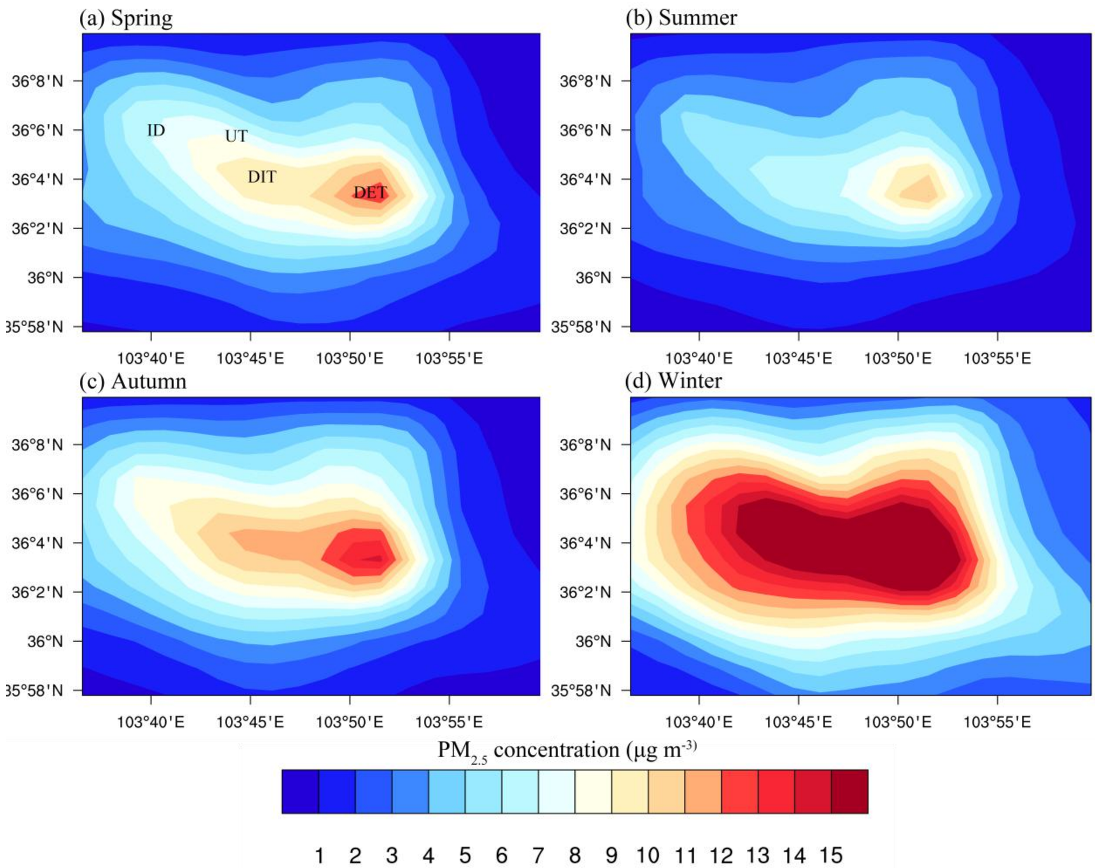

Figure S4 The spatial distributions of simulated FRD PM2.5 concentrations in (a) spring, (b) summer, (c) autumn and (d) winter based on the WRF-Chem model.